Electronic structure and magnetic properties of 3d impurities in antiferromagnetic Cr

2008 J. Phys.: Condens. Matter 20 285204

(http://iopscience.iop.org/0953-8984/20/28/285204)

J. Phys.: Condens. Matter **20** (2008) 285204 (8pp) doi:10.1088/0953-8984/20/28/285204

Electronic structure and magnetic properties of 3d impurities in antiferromagnetic Cr

S N Mishra[1] **and S K Srivastava**[2]

[1] Department of Nuclear and Atomic Physics, Tata Institute of Fundamental Research, Homi Bhabha Road, Mumbai-400005, India
[2] Department of Physics and Meteorology, Indian Institute of Technology, Kharagpur-721302, India

E-mail: mishra@tifr.res.in and sanjeev@phy.iitkgp.ernet.in

Received 21 February 2008, in final form 22 May 2008
Published 13 June 2008
Online at stacks.iop.org/JPhysCM/20/285204

Abstract

Using the full-potential linearized augmented plane wave (FLAPW) method based on the density function theory (DFT) we have performed *ab initio* calculations of magnetic properties for dilute Cr–X alloys with 3d transition metals. We present here our results for the density of states, local magnetic moments and hyperfine fields. The paramagnetic local density of states (LDOS) analyzed with the Stoner model suggests the occurrence of local moments for Mn, Fe, Co and Ni consistent with results obtained from spin polarized calculations. In addition, we find a large magnetic moment for the non-magnetic V atom in Cr. The impurity moments of Sc, Ti, V and Mn are found to be antiparallel with respect to the near neighbor Cr moment while, they show ferromagnetic coupling for Fe, Co, and Ni. The observed sign change for the exchange coupling is also reflected in our calculated hyperfine field results. The trend observed for the variation of the impurity moment and hyperfine fields of 3d impurities in antiferromagnetic Cr show remarkable similarity with the results reported for ferromagnetic Fe, Co and Ni hosts. The results presented here would be helpful for a common understanding of local magnetic properties of transition metal impurities in ferro and antiferromagnetic hosts.

1. Introduction

Local magnetism of transition metal impurities in simple ferro and antiferromagnetic hosts constitutes an important area of research in condensed matter physics. While extensive studies, both experimental and theoretical, have been made to study the magnetic behavior of 3d and 4d impurities in elemental ferromagnets like Fe, Co and Ni [1–7] very few studies have been made in elemental antiferromagnets like Cr and Mn. Chromium is one of the most interesting elements of the periodic table because of its unique magnetic properties. It shows incommensurate spin-density wave (SDW) antiferromagnetic behavior with a Neel temperature $T_N = 311$ K, originating from nesting properties of the Fermi surface [8]. It also undergoes an order–order transformation at 123 K with a change of spin orientation and the magnetic wavevector. The magnetic wavevector has also been found to change dramatically by alloying with other elements resulting in a crossover over from an incommensurate to commensurate antiferromagnetic structure [9]. Apart from many interesting physics issues related to magnetism, chromium alloys are also useful for shape-memory and high temperature applications. As such, investigations of chromium alloys, especially their magnetic properties continue to be a subject of intense experimental and theoretical study. Over the years, extensive experimental data have been compiled on the magnetic behavior of Cr alloys with 3d and 4d elements. The results have revealed that the magnetic moment, as well as the transition temperature, either increase or decreases depending on the type of impurity. While, elements to the left of Cr in the periodic table decrease the moment and T_N, impurities to its right show the opposite effect. Compared to the experimental situation, very few theoretical studies on magnetic behavior of dilute Cr alloys with transition metals have been carried out. As far as we know, only two such investigations have been reported in the literature. Using the linear-muffin-tin-orbital

(LMTO) method Antropov *et al* have studied the magnetism of 3d impurities (V–Ni) in Cr showing large magnetic moments for Fe and Co [10]. Recently, Hashemifar *et al* have reported the magnetic moment and hyperfine field of several impurities in Cr including Fe, Ru, Rh and Pd [11]. Due to lack of experimental or theoretical results for the local moments and hyperfine fields of transition metal impurities in Cr, any systematic trend in their behavior have not been established so far.

In this paper we present detailed *ab initio* calculations of the magnetic moment and hyperfine fields of 3d impurities (Sc–Ni) in antiferromagnetic Cr. The calculations have been performed within the generalized gradient approximation of density functional theory (DFT). The variation of local moments and hyperfine fields across the 3d series show remarkable similarity with those observed for ferromagnetic hosts such as Fe, Co and Ni. In addition, the variations in impurity induced changes in the calculated alloy moment qualitatively agree with the experimental results obtained from bulk magnetization measurements. The results presented in this work would be helpful for a common understanding of local magnetic properties of transition metal impurities in ferro and antiferromagnetic hosts.

2. Calculation details

The calculations presented in this paper have been performed within the framework of density functional theory [12, 13] using the all-electron full-potential linearized augmented plane wave (FP-LAPW) method as implemented in the WIEN2k package [14, 15]. To achieve the representative condition of sufficiently dilute Cr–X alloys, a cubic supercell consisting of 27 bcc chromium unit cells having 54 atoms was constructed by repeating the unit cell three times in x, y, and z directions ($3 \times 3 \times 3$). The Cr atom at the origin (0, 0, 0) of the supercell was replaced by the impurity atom. The unit cell thus constructed represents a Cr–X alloy of composition $Cr_{0.9815}X_{0.0185}$. In such a unit cell there are eight non-equivalent atoms with lattice positions: Cr0/X (0, 0, 0); Cr1(1/6, 1/6, 1/6), Cr2(1/3, 0, 0), Cr3(1/3, 1/3, 0), Cr4(1/2, 1/6, 1/6), Cr5(1/3, 1/3, 1/3), Cr6(1/2, 1/2, 1/6) and Cr7/X(1/2, 1/2, 1/2). The labels for the Cr atoms are arranged according to their distance from the origin/impurity with Cr1 being the closest and Cr7 as the farthest. For the supercell used for our studies, the impurity atoms are well separated so that the impurity–impurity interaction can be considered to be small.

In the FLAPW method, the unit cell is divided into two regions: (i) non-overlapping muffin-tin spheres of radius R_{MT} around each atom and (ii) the remaining interstitial region. For the wavefunctions inside the atomic spheres, a linear combination of radial function times spherical harmonics are used, while in the interstitial region a plane wave expansion is used. In our calculations, we have used R_{MT} values of 2.25 au for Cr and 2.28–2.4 au for the impurity atoms. The maximum multipolarity l of the wavefunctions inside the atomic sphere was restricted to $l_{max} = 10$. The wavefunctions in the interstitial region were expanded in plane waves with a cutoff of $k_{max} = 7.5/R_{MT}^{min} = 3.33$ au^{-1}. The charge density was Fourier expanded up to $G_{max} = 14\ \sqrt{Ry}$. For the exchange correlation potential, we used the Perdew–Burke–Ernzerhof (PBE) formalism of the generalized gradient approximation (GGA) [16]. For sampling of the Brillouin zone, a k-mesh with 35 special k-points in the irreducible zone (IBZ) was used. All calculations were performed using the equilibrium lattice parameters obtained by calculating the total energy at different volumes and fitting the results to the Birch–Murnaghan equation of state [17] implemented within Wien2k program [14]. Due to lattice imperfection caused by the impurity, the atoms at their ideal positions experience a non-zero force which must be minimized to obtain the self-consistent converged solution. This was achieved by allowing the atoms to relax to new positions until the force reduced to less than 1 mRy au^{-1}. For all the cases studied here, calculations were performed with and without spin polarization, the latter being useful for extracting information related to local moment formation on the impurity. For the spin polarized case, calculations were performed using the commensurate antiferromagnetic structure of Cr in which the magnetic moments for atoms 1, 4, 6, 7 were considered to be parallel with respect to an arbitrarily defined magnetic field direction while, the moments of the atoms 0, 2, 3 and 5 were taken as being antiparallel. For the cases of Mn, Fe, Co and Ni calculations were also performed by flipping the impurity spin direction and the self-consistent ground state was determined by comparing the total energy of the two spin configurations.

3. Results and discussion

3.1. Structural properties

The calculated structural properties e.g. equilibrium lattice constants, near neighbor distances, cohesive energies defined as $E_c = E_{alloy} - \sum E_{Atom}$ with E_{tot} and E_{Atom} being the self-consistent total energy of the supercell and energies of isolated atoms, and the bulk moduli of Cr–X alloys (X = Sc–Ni) are summarized in table 1. The bulk moduli were obtained by fitting the total energy of the supercell at different volumes to the Birch–Murnaghan equation of state [17]. For pure Cr, our results closely agree with the values reported in the literature [11, 18]. In all the cases studied, the lattice constant a(Å) was found to decrease with the atomic number of the impurity atom X, while the bulk modulus and the cohesive energy peaks near the middle of the 3d series suggest a lowering of bond strength on either end.

3.2. Density of states and specific heat

Figure 1 displays the impurity projected local density of states (LDOS) for 3d impurities in Cr obtained from unpolarized as well as spin polarized calculations. Let us first look at the LDOS results from the non-magnetic (unpolarized) calculations. Starting with the case of pure Cr, the calculated LDOS exhibits the typical three peak structure of bcc metals with the Fermi energy falling in a pseudo-gap separating the lower-lying bonding states from the higher anti-bonding ones. The calculated Fermi energy E_F and the density states at E_F for

Table 1. Summary of calculated structural properties of Cr–X alloys with different 3d impurities X = Sc–Ni. a (Å): equilibrium lattice constant of the unit cell; d_{nn} (Å): near neighbor distance; E_c (Ry): cohesive energy per unit of $Cr_{53}X$; and B (GPa): bulk modulus.

Impurity X	a	d_{nn}	E_c	B
Cr (pure)	8.628	2.491	−17.65	190
Sc	8.673	2.504	−16.99	179
Ti	8.642	2.495	−17.18	183
V	8.623	2.489	−17.34	187
Mn	8.609	2.485	−17.68	191
Fe	8.591	2.480	−17.36	187
Co	8.583	2.478	−17.27	185
Ni	8.595	2.482	−17.06	181

paramagnetic Cr come out to be 0.759 Ry and 0.697 states/ev-atom respectively which, agree with the values reported in literature [19]. In the case of Cr–X alloys, in the features observed in LDOS of the impurity atoms, though qualitatively similar to Cr, one can easily notice impurity dependent differences with respect to the positions of the bonding and anti-bonding states relative to E_F. While the centroid of the bonding states do not show much change, the position of the anti-bonding peaks significantly vary with respect to the atomic number Z_{imp} of the impurity. Beginning with X = Sc, with increasing Z_{imp} the anti-bonding peak progressively moves to closer to E_F. For the heavier impurities Mn, Fe, Co and Ni the anti-bonding states appear as a sharp resonance—virtual bound state (VBS)—passing through the E_F between Fe and Co. This leads to a large enhancement in the density of states at the Fermi energy $N(E_F)$ which was estimated to be 1.2, 3.0, 2.6 and 1.7 states/eV-atom for Mn, Fe, Co and Ni respectively. For the early impurities the $N(E_F)$ value come out to be $\leqslant$0.6 states/eV-atom. Figure 2 shows the variation of $N(E_F)$ in Cr–X alloys with X = Sc–Ni. Applying Stoner criteria [20]: $IN(E_F >)1$, one can find if the formation of local moment for 3d impurities in Cr is possible or not. Here, I is the well known Stoner exchange parameter. Using $I = 0.9$ eV known for 3d impurities respectively, [20] the critical value of $N(E_F)$ above which an intrinsic local moment on the impurity is likely to form in Cr matrix comes out to be 1.08 states/eV-atom for 3d and 1.67 states/eV-atom for 4d impurity atoms. Examining the results shown in figure 2 it can be seen that the Stoner condition for local moment formation in Cr host is satisfied for Fe, Co and Ni while, in the case of Mn the $N(E_F)$ value falls close to the Stoner limit which indicates that the magnetic moment of Mn in Cr is likely to be unstable. It should be mentioned here that the predicted moment instability for Mn in Cr is born out in our spin polarized calculations where we observe two different stable solutions having similar total energies but opposite spin alignment. For all other cases studied here, the $N(E_F)$ falls below the critical value which suggests that the moments of these impurities, are most likely induced by the surrounding magnetic Cr atoms.

We now examine the results obtained from the spin polarized calculations. Starting with pure Cr, the LDOS for the majority as well as the minority-spin states exhibit the typical pseudo-gap structure yielding a magnetic moment of 1.19 μ_B which, agrees with the values reported from earlier

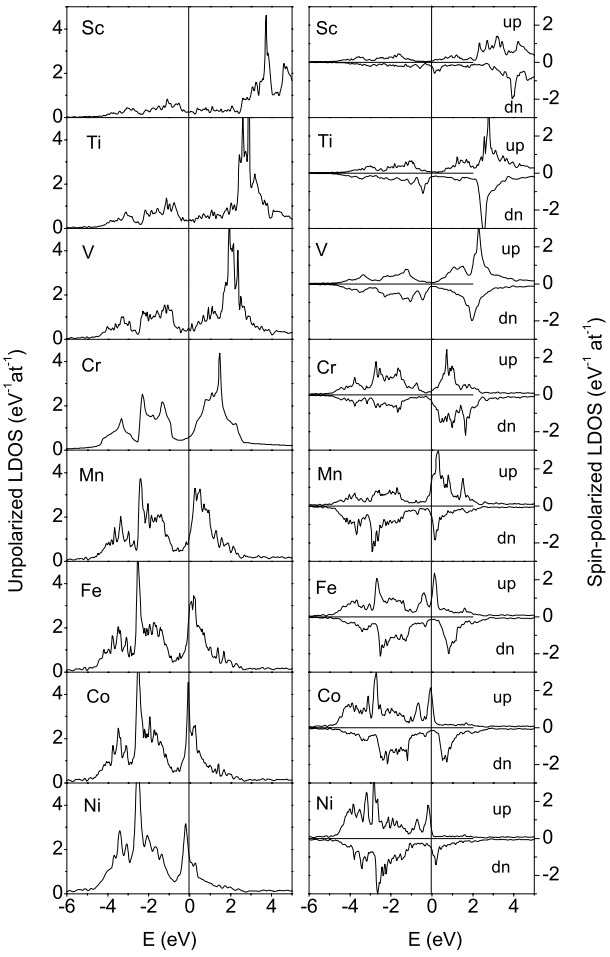

Figure 1. Local density of states for 3d impurities in Cr. Panel on the left corresponds to unpolarized LDOS while the right panel is for spin polarized cases. The Fermi energy E_F is shown as a vertical solid lines passing through the zero of the energy axis.

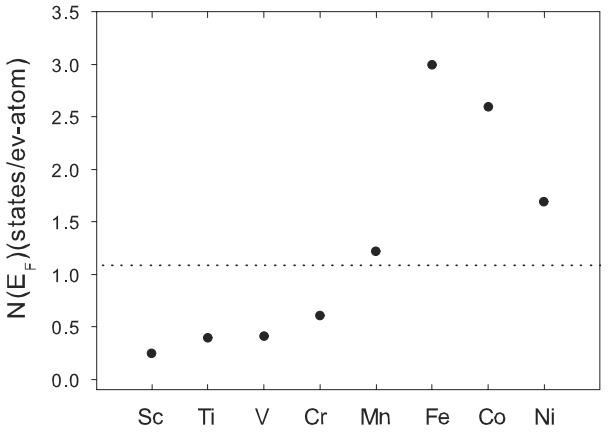

Figure 2. Non-magnetic local density of states at the Fermi energy for different 3d impurities in Cr. The dotted line represents the Stoner limit for moment formation.

calculations [11, 18, 21–23]. The calculated moment of Cr, however, turns out to be higher than the experimental value reported from neutron diffraction measurements [8]. Cottenier

Table 2. Summary of calculated magnetic properties of $Cr_{53}X$ (X = Sc–Ni). M_0 (μ_B): local magnetic moment of the impurity X; δM_n (μ_B): change in Cr magnetic moment for the seven near neighbor shells around the impurity; and ΔM (μ_B): change in net magnetic moment of the unit cell.

X	M_0	δM_1	δM_2	δM_3	δM_4	δM_5	δM_6	δM_7	ΔM
Sc	0.050	−0.126	+0.007	−0.035	+0.001	−0.021	−0.005	−0.012	−0.442
Ti	−0.158	−0.116	+.006	−0.029	+0.002	−0.019	−0.005	−0.01	−0.376
V	−0.704	−0.071	+0.009	−0.023	+.004	−0.012	+.002	−0.008	−0.348
Cr	−1.190	0	0	0	0	0	0	0	0.0
Mn	−1.466	+0.028	−0.018	+.012	−0.010	+0.005	−0.004	+0.001	0.433
Fe	0.217	−0.054	+0.008	−0.024	+0.001	−0.014	−0.004	−0.01	0.167
Co	0.901	0.011	−0.014	+0.005	−0.009	+.001	−0.005	−0.002	0.221
Ni	0.546	−0.025	−0.004	−0.012	−0.006	−0.010	−0.008	−0.009	0.067

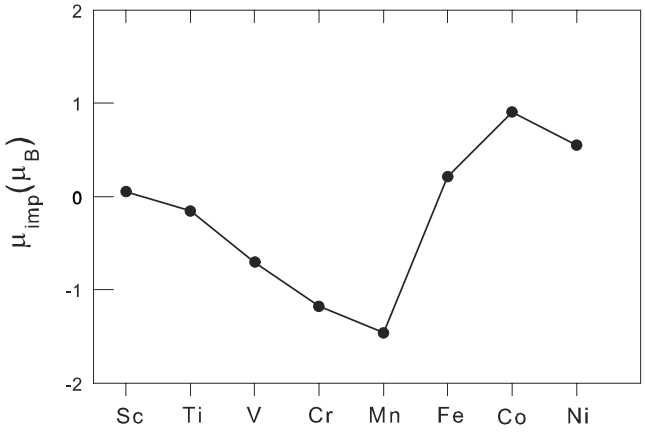

Figure 3. Local magnetic moments of 3d impurities in a Cr host.

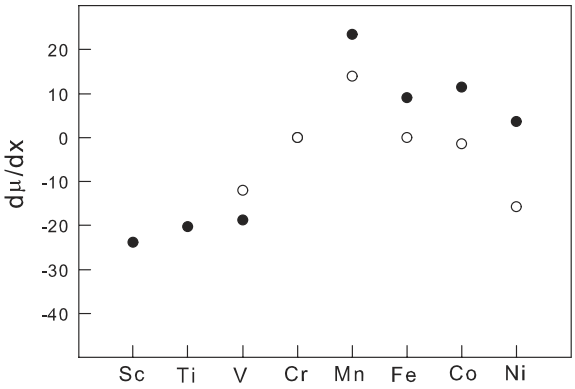

Figure 4. Moment change per impurity atom ΔM for dilute Cr–X alloys; X = Sc–Ni. Filled symbols: present calculations; open symbols: experimental data taken from [9].

et al [18] have shown that the magnetic moment of Cr in the antiferromagnetic phase is sensitive to the exchange correlation potential used. While GGA calculations overestimates the magnetic moment with respect to the experimental value, LDA is unable to find a stable AF ground state for Cr [21–23]. We would like to emphasize that this difference in the absolute value of Cr magnetic moment does not influence the main conclusion of this paper.

Coming to the Cr–X alloys, for the early impurities Sc, Ti, V the local DOS show the formation of unoccupied virtual bound states (VBS) for both the spin directions which progressively moves closer to the Fermi energy with an increase of atomic charge. In the case of Mn, we find a sharp resonance—virtual bound state—in the minority-spin band just above E_F. In addition, a broader VBS is also seen in the majority-spin band at ≈0.4 eV above E_F. Going further down in the series, the situation is different for Fe, Co and Ni. Here, the VBS is visible in the majority-spin band well separated from the unoccupied peak in the minority-spin band. The VBS in the majority-spin band passes through E_F between Fe and Co consistent with the features observed in the non-magnetic DOS discussed above. The above feature reflects that the coupling between the moments of the impurity and near neighbor Cr atoms changes sign between Mn and Fe. This is also manifested in the self-consistent moment values estimated by integrating the DOS below E_F, as discussed later. Here, it should be mentioned that for Mn we also find a stable solution with ferromagnetic coupling with slightly higher (≈1 mRy) total energy compared to the ground state with AF coupling. This suggests that Mn in Cr is close to a magnetic instability which is consistent with the prediction made from Stoner analysis of the unpolarized DOS results discussed above. It is worthwhile noting that a multiplicity of magnetic solutions have also been reported for Mn and Fe impurities on the Fe(001) surface [24].

3.3. Magnetic moments

The calculated magnetic moments for the 3d impurity atoms in Cr are summarized in table 2. Figure 3 shows the variation of impurity local moment across the 3d series. It can be noticed that 3d impurities like V, Mn, Co and Ni in Cr show large magnetic moments with magnitudes −0.70 μ_B, −1.47 μ_B, 0.90μ_B and 0.55 μ_B respectively. On the other hand, the magnetic moment of Fe in Cr come out to be rather small ≈0.22 μ_B. Particularly noteworthy is the observation of a large magnetic moment for the non-magnetic atom V which is supported by the effective moment ≈1 μ_B/V obtained from measurements of bulk magnetic susceptibility of dilute $Cr_{1-x}V_x$ alloys [25]. The calculated low magnetic moment of Fe in Cr is consistent with the results reported from Mössbauer and perturbed angular distribution (TDPAD) studies [27–29], but differ from the moment values μ_{Fe} = 1.7–3.1 μ_B obtained from bulk susceptibility measurements in dilute $Cr_{1-x}Fe_x$ alloys [9, 26]. Similarly, the calculated moment of Co impurities are lower compared to the values

$\mu_{Co} = 1.7$–$2.9\ \mu_B$ reported from macroscopic magnetization studies [9]. Theoretically, the magnetic behavior of 3d impurities in antiferromagnetic Cr host was earlier calculated by Antropov *et al* [10] using LMTO-ASA method. The moment values for V, Mn, Fe Co and Ni were reported to be 0.36 μ_B, 0.48 μ_B, $\approx\pm 2\ \mu_B$, $-1.6\ \mu_B$ and $-0.13\ \mu_B$ respectively. Recently, using a 16 atom supercell ($-Cr_{15}Fe$) and the FLAPW method Hashemifar *et al* [11] calculated the magnetic moment of Fe in Cr to be $-0.61\ \mu_B$. They also reported an energetically close ferromagnetic solution with an Fe moment of $1.81\ \mu_B$. Our moment values significantly differ from these results, especially for Fe, Co and Ni. We believe this difference is mainly due to larger impurity concentrations corresponding to the smaller ($2 \times 2 \times 2$) supercell used in the previous calculations. Later, we shall illustrate the concentration dependence by comparing results obtained from our calculations made for a few cases of $Cr_{0.9815}X_{0.0185}$ ($3 \times 3 \times 3$ supercell with 54 atoms) and $Cr_{0.9375}X_{0.0625}$ ($2 \times 2 \times 2$ supercell with 16 atoms). The trends observed for the 3d impurity moments in antiferromagnetic Cr are qualitatively similar to those reported for ferromagnetic hosts Fe, Co and Ni [2–7].

The impurity atoms also results in a strong perturbation of the host-Cr magnetic moments. The calculated moment change δM_n ($n = 1, 2, \ldots, 7$) for Cr atoms in the first seven near neighbor shells around the impurities are listed in table 2. With increasing distance from the impurity site, the δM values decrease and show the typical Friedel like oscillation. Summing the δM values for all the atoms in the unit cell, including the impurity shell one can obtain the net change in magnetization $\Delta M = \delta M - M_{imp} + M_{Cr}$. Taking the impurity concentration to be $x = 0.0185$ for the $3 \times 3 \times 3$ supercell, the calculated change in magnetization per impurity atom for the Cr–X alloys can be compared with the $d\mu/dx$ values measured experimentally. The results are shown in figure 4 along with available experimental data. It is satisfying to note that our calculated results qualitatively reproduce the experimentally observed trend [9].

3.4. Hyperfine fields

In addition to the magnetic moments discussed above we have calculated the hyperfine fields (HF) of 3d impurities in a Cr host to examine their magnetic behavior at a microscopic level. The hyperfine field generally has contributions from dipolar, orbital and Fermi contact interactions. For the cases studied here, because of the cubic point symmetry, the orbital and dipolar fields are negligibly small. The dominant contribution to HF thus arises from Fermi contact interaction which depends on the s-electron spin density at the nuclear site $n^s(0)$. The HF values were calculated using the scalar relativistic formula [6]

$$B_{hf} = (8\pi/3)\mu_B m_{av};\ m_{av} = \int^{E_F} dE\,[F_0^+(E)n_0^+(E) - F_0^-(E)n_0^-(E)] \quad (1)$$

implemented within the Wien2k program [14]. Here, m_{av} is the average magnetic moment near the nucleus and $F_0^{\pm}(E)$ are the relativistic correction factors [6]. The results are displayed in figure 5 and summarized in table 3. Also shown are the results for the core and valence contributions (B_{hf}^{core} and B_{hf}^{val}) to the HF values. For the 3d impurities, the magnitudes of the core and valence hyperfine fields B_{hf}^{core} and B_{hf}^{val}, opposite in sign, increase from Sc to Mn and then decrease for Fe, Co and Ni. The two contributions cancel in between Mn–Fe resulting in a change of sign for the total hyperfine field B_{hf}^{tot}. The variation of B_{hf}^{tot} is similar to the trend observed for the impurity local moment (see figure 4). The calculated total HF values agree with experimental results available for Fe in Cr [1, 27–29]. In particular, we like to point out that our result for Fe in Cr ($Cr_{53}Fe$) shows excellent agreement with the experimental data as compared to the results reported by Hashemifar *et al* [11] which was obtained for $Cr_{15}Fe$. This discrepancy once again suggests that impurity–impurity interaction plays a significant role on the magnetic behavior of Cr–X alloys—a point we shall discuss later.

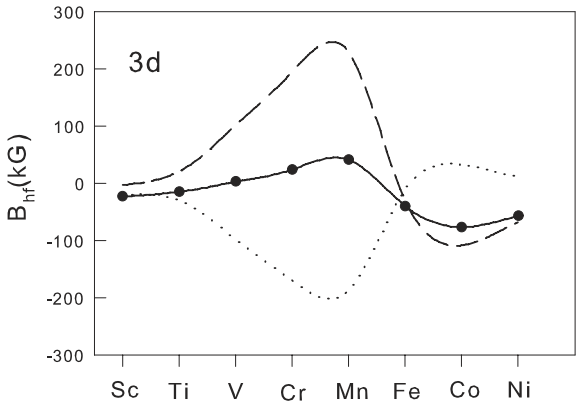

Figure 5. Magnetic hyperfine fields of 3d impurities in Cr host. The symbols and solid line represent the total hyperfine field B_{hf}^{tot}. The dotted and dashed lines represent the core and valence contributions, respectively.

Table 3. Summary of the calculated magnetic hyperfine fields of 3d impurities in antiferromagnetic Cr host. B_{hf}^{tot} (kG) denotes the total hyperfine field, while B_{hf}^{core} (kG) and B_{hf}^{val} (kG) are the core and valence contributions, respectively. The last column shows the total hyperfine field for the nearest neighbor Cr atom.

Impurity	B_{hf}^{tot}	B_{hf}^{core}	B_{hf}^{val}	B_{hf}^{tot} (Cr-1nn)
Sc	−23.51	−3.18	−20.33	14.17
Ti	−15.24	20.40	−30.64	16.64
V	2.66	114.19	−116.85	−17.07
Cr (pure)	23.71	194.46	−170.75	23.71
Mn	41.10	229.22	−188.12	27.89
Fe	−40.67	−23.97	−16.70	20.58
Co	−76.99	−108.76	31.77	25.88
Ni	−57.38	−67.82	−10.44	21.7

Next we discuss the individual contributions to the hyperfine fields, i.e. the core and valence contributions B_{hf}^{core} and B_{hf}^{val} which are listed in table 3. For magnetic impurities B_{hf}^{core} is large because of exchange interaction of the polarized d-shell with the core s-orbitals. In general, B_{hf}^{core} scales with the local moment of the impurity and has the opposite sign. The valence contributions to the hyperfine fields B_{hf}^{val} are more complicated. It has two major contributions: (i) from the

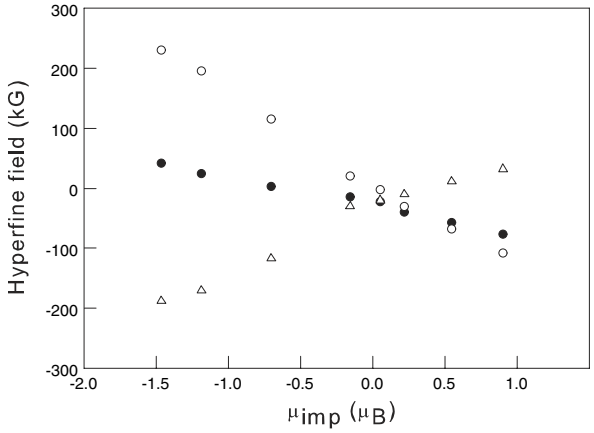

Figure 6. Variation of hyperfine fields as a function of impurity local moment for 3d impurities in Cr host. ●: $B_{\rm hf}^{\rm tot}$; ○: core hyperfine field and △: valence contribution to HF.

polarization of outer s-orbitals of the impurity by its own local moment and (ii) polarization of valence electrons due to the magnetic moments of the neighboring host atoms. The later, known as the transferred field is usually proportional to the magnetic moments of the surrounding host atoms and positive with respect to its direction. Figure 6 displays the variation of $B_{\rm hf}^{\rm tot}$, $B_{\rm hf}^{\rm core}$ and $B_{\rm hf}^{\rm val}$ with respect to the impurity local moment. It can be seen that the HF values scale with the impurity local moment yielding hyperfine coupling constants: $A_{\rm core} = -140$ kG/$\mu_{\rm B}$; $A_{\rm val} = +90$ kG/$\mu_{\rm B}$ and $A_{\rm tot} = -50$ kG/$\mu_{\rm B}$. These values are comparable to the results reported for 3d impurities in ferromagnetic Fe, Co and Ni hosts [2–4, 6]. Looking at the results shown in figure 6, the observed proportionality between $B_{\rm hf}$ and the impurity moments suggests that the hyperfine fields of 3d and 4d impurities in Cr is dominated by the local contributions with relatively weak transferred field from the neighboring Cr atoms.

For further analysis of the different contributions to the total hyperfine field at the impurity site, following Blügel *et al* [6] we write

$$B_{\rm hf}^{\rm tot} = aM_{\rm loc} + bM_{\rm host} + c\sum_{i=NN}\delta M_i \qquad (2)$$

where, the first term represents the local hyperfine field of the impurity, being the sum of the local core and valence contributions, which are proportional to the local moment of the impurity. The second and third terms represent the transferred hyperfine field consisting of a constant contribution $bM_{\rm host}$ and a correction $c\sum_{i=NN}\delta M_i$ due to impurity induced perturbations in the magnetic moments of neighboring host atoms. Using the calculated values for $\Delta M = {\rm sum}_{i=1\ldots7}\delta M_i$, the $B_{\rm hf}^{\rm tot}$ shown in table 2 could be fitted reasonably well with the constants a, b and c as:

$a \approx -50$ kG/$\mu_{\rm B}$; $b \approx -20$ kG/$\mu_{\rm B}$ and $c \approx -10$ kG/$\mu_{\rm B}$ for 3d impurities.

The above analysis, although does not accurately reproduce the HF values for all the cases studied, it shows the trend that the transferred component is relatively weak compared to the local contribution.

Table 4. Summary of calculated magnetic properties of $Cr_{53}X$ (X = Sc–Ni) obtained at different lattice constants. $M_{\rm imp}$ ($\mu_{\rm B}$): magnetic moment at the impurity atom X; $\mu_{\rm Cr-1}$ and $\mu_{\rm Cr-7}$: moments on the Cr atoms closest to and farthest from the impurity, respectively; ΔM ($\mu_{\rm B}$): change in unit cell moment and $B_{\rm hf}$ (kG): total hyperfine field at the impurity site.

Impurity	Lattice constant	$M_{\rm imp}$	$\mu_{\rm Cr-1}$	$\mu_{\rm Cr-7}$	ΔM	$B_{\rm hf}$
Sc	2.74	0.0	0.08	0.12	−0.37	−2.3
	2.81	0.01	0.58	0.67	−0.25	−9.8
	2.88	0.03	1.06	1.18	−0.41	−25.2
Ti	2.74	−0.03	0.07	0.12	−0.28	−1.5
	2.81	−0.07	0.62	0.68	−0.21	−6.7
	2.88	−0.16	1.07	1.18	−0.38	−15.3
V	2.74	−0.05	0.09	0.11	−0.22	−0.4
	2.81	−0.30	0.63	0.68	−0.26	1.9
	2.88	−0.71	1.08	1.18	−0.34	4.4
Cr	2.74	−0.13	0.13	0.13	0	0.3
	2.81	−0.69	0.69	0.69	0	12.3
	2.88	−1.19	1.19	1.19	0	22.9
Mn	2.74	−0.26	0.14	0.11	0.33	4.1
	2.81	−0.82	0.70	0.67	0.24	18.4
	2.88	−1.51	1.22	1.19	0.46	41.9
Fe	2.74	0.89	0.15	0.12	0.41	−47.1
	2.81	0.44	0.71	0.65	0.29	−46.0
	2.88	0.21	1.14	1.18	0.16	−37.8
Co	2.74	0.99	0.16	0.11	0.57	−67.3
	2.81	0.95	0.73	0.68	0.26	−82.0
	2.88	0.89	1.20	1.17	0.31	−107.5
Ni	2.74	−0.01	0.10	0.13	−0.13	−0.8
	2.81	0.27	0.70	0.62	−0.17	−45.9
	2.88	0.59	1.16	1.18	0.12	−63.6

At this point it is important to discuss possible variations in the magnetic properties of the impurity atoms due to small changes in electronic structure of the Cr host. As mentioned before, the electronic structure and magnetic moment of bcc Cr sensitively depends on the exchange correlation function used. While GGA calculations correctly predict the structural properties the magnetic moment of antiferromagnetic Cr come out to be much higher than the experimental value. Furthermore, within GGA formalism, the magnetic moment of antiferromagnetic Cr has been shown to change with slight variation of the lattice parameter a—decreasing from 1.19 $\mu_{\rm B}$ at the equilibrium value of $a = 2.876$ Å to almost zero below $a = 2.74$ Å [18]. The calculated magnetic moment of Cr was found to agree with the experimental value for $a = 2.81$ Å. To study the dependence of $\mu_{\rm imp}$ and $B_{\rm hf}$ on host-Cr magnetism, we have performed supercell calculations ($3 \times 3 \times 3$) for all the cases reported above using lattice parameters $a = 2.74$, 2.81 and 2.88 Å, the latter being the experimental value. The results are shown in figure 7 and summarized in table 4.

Let us first look at the results for pure Cr. With decreasing lattice constant (inter-atomic distance), due to increased hybridization, the 3d-bands of Cr become broad (see figure 7(a)) and the magnetic moment decrease rapidly from 1.19 $\mu_{\rm B}$ at 2.88 Å to 0.13 $\mu_{\rm B}$ at 2.74 Å consistent with the results reported by Cottenier *et al* [18]. Concomitant with the reduction of host-Cr moment, the impurity atoms, except Fe

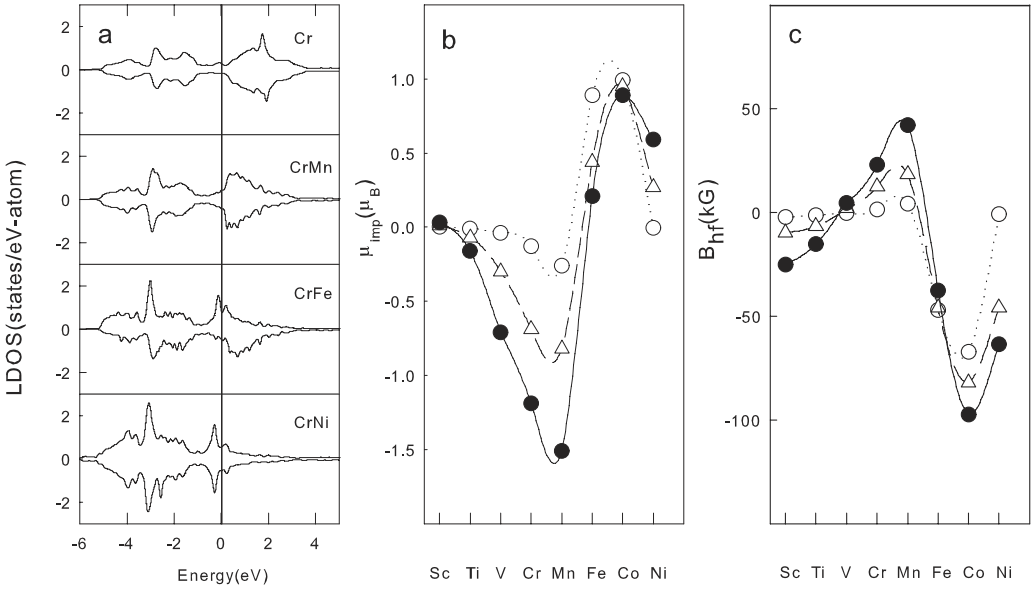

Figure 7. Calculated magnetic properties of $Cr_{53}X$ (X = Sc–Ni): (a) spin resolved LDOS of Mn, Fe and Ni impurities in Cr calculated at lattice constant $a = 2.74$ Å; (b) impurity magnetic moment and (c) hyperfine field of 3d impurity atoms at lattice constants, $a = 2.88$ Å (●; solid line); $a = 2.81$ Å (△; dashed line); $a = 2.74$ Å (○; dotted line).

Table 5. Magnetic moments and hyperfine fields calculated for $Cr_{15}X$ (X = Sc–Ni). μ_{imp}: impurity magnetic moment in μ_B; B_{hf}^{tot}: total magnetic hyperfine field in kG.

	Sc	Ti	V	Cr	Mn	Fe	Co	Ni
μ_{imp}	+0.04	−0.15	−0.57	+1.18	−1.60	+0.59	+1.08	+0.64
B_{hf}^{tot}	−15.7	−1.35	+3.66	+23.51	+35.92	−68.51	−100.85	−80.43

and Co, show a tendency to lose their magnetic moment. In the cases of Fe and Co, however, a reduction of lattice resulted in an increase of the magnetic moment mainly because of the majority-spin bands being pushed below the Fermi energy (see figure 7(a)). Moving further down in the series to Ni, both majority and minority-spin bands of the impurity atom move below the Fermi energy and their relative populations become equal at $a = 2.74$ Å leading to a vanishing magnetic moment. It is worth while mentioning that unpolarized calculation for $Cr_{53}Ni$ at 2.74 Å yielded $N(E_F) = 1.0$ states/eV-atom which is lower than the Stoner limit for moment formation (see figure 2). Here, we also emphasize that the variation in lattice constant, although it results in a significant change in the μ_{imp} and B_{hf} values, does not alter the general trend observed at the equilibrium lattice constant (see figures 3 and 5).

3.5. Concentration dependence

Finally we come to discuss the influence of impurity concentration on the magnetic moment as well as hyperfine fields. For this, we compare the results calculated for $Cr_{53}X$ ($3 \times 3 \times 3$ supercell) and $Cr_{15}X$ ($2 \times 2 \times 2$ supercell). The two supercells are equivalent to Cr–X alloys with the concentration of X being 0.0185 and 0.0625 respectively. For the $2 \times 2 \times 2$ supercell calculations we used the lattice parameters shown in table 1, scaled by a factor 2/3 to account for the difference in supercell size. The Brillouin zone integration in this case was done with a finer k-mesh consisting of 84-k points in the irreducible zone. The calculated impurity magnetic moments and the hyperfine field values are listed in table 5.

The moment values obtained from our $2 \times 2 \times 2$ supercell calculations closely agree with the results reported by Antropov *et al* [10] and Hashemifar *et al* [11]. It should also be mentioned that apart from the minimum energy spin configuration mentioned in table 4, we also obtain a ferromagnetic solution for Mn with a moment of 2.04 μ_B with slightly higher energy (≈1 mRy). Similarly, for Fe we get an antiferromagnetic solution with a moment of 1.94 μ_B with total energy 4 mRy higher than the ferromagnetic solution. These observations are consistent with the results reported earlier [10, 11]. Comparing the results of $Cr_{15}X$ (table 4) with the values calculated for $Cr_{53}X$ (tables 2 and 3) it can be clearly noticed that the magnitude of impurity local moment and the related hyperfine field is substantially different for V, Mn, Fe, Co and Ni. For 4d impurities, however, the size of the supercell did not have much influence on the magnetic properties. The results thus demonstrate that impurity–impurity interaction plays an important role on the local magnetic properties of 3d impurities in Cr host, particularly for the cases of Mn, Fe and Co.

In summary, using the full-potential linearized augmented plane wave (FLAPW) method based on the density function theory (DFT) we have made *ab initio* calculations for the magnetic properties of dilute Cr–X alloys with 3d transition

metals. The calculated results show excellent agreement with available experimental data. The trends observed for the magnetic moment and hyperfine field of 3d impurities in antiferromagnetic Cr show remarkable similarity with those in ferromagnetic Fe, Co and Ni hosts. The results presented in this work provide a basis for a comprehensive understanding of magnetic and electronic properties of dilute Cr alloys. The results presented in this work would be helpful for a common understanding of local magnetic properties of transition metal impurities in ferro and antiferromagnetic hosts.

References

[1] Rao G N 1985 *Hyperfine Interact.* **24–26** 1119 and references therein
[2] Akai H, Akai M and Kanamori J 1985 *J. Phys. Soc. Japan.* **54** 4257
[3] Drittler B, Stefanou N, Blügel S, Zeller R and Dederichs P H 1989 *Phys. Rev.* B **40** 8203
[4] Stepanyuk V S, Zeller R, Dederichs P H and Mertig I 1994 *Phys. Rev.* B **49** 5157
[5] Paduani C 2004 *J. Magn. Magn. Mater.* **278** 76
[6] Blügel S, Akai H, Zeller R and Dederichs P H 1987 *Phys. Rev.* B **35** 3271
[7] Zeller R 1987 *J. Phys. F: Met. Phys.* **17** 2123
[8] Fawcett E 1988 *Rev. Mod. Phys.* **60** 209
[9] Fawcett E, Albetrs H L, Galkin V Yu, Noakes R R and Yakhami J V 1994 *Rev. Mod. Phys.* **66** 25
[10] Antropov V P, Anisimov V I, Liechtenstein A I and Postnikov A V 1988 *Phys. Rev.* B **37** 5603
[11] Hashemifar S J, Ghaderi N, Sirousi S and Akbarzadeh H 2006 *Phys. Rev.* B **73** 165111
[12] Hohenberg P and Kohn W 1964 *Phys. Rev.* **136** 864
[13] Kohn W and Sham L J 1965 *Phys. Rev.* **140** A1133
[14] Blaha P, Schwarz K, Madsen G, Kvasnicka D and Luitz J 1999 *WIEN2k an Augmented Plane Wave + Local Orbitals Programm for Calculating Crystal Properties* Karlheinz Schwarz, Techn. Universitat Wien, Austria ISBN 3-9501031-1-2
[15] Cottenier S 2002 *Density Functional Theory and the Family of (L)APW-methods: A Step-By-Step Introduction* (K.U.Leuven, Belgium: Instituut voor Kern-en Stralingsfysica) ISBN 90-807215-14
[16] Perdew J P, Burke K and Ernzerhof M 1996 *Phys. Rev. Lett.* **77** 3865
[17] Birch F 1947 *Phys. Rev.* **71** 809
Murnaghan F D 1951 *Finite Deformation of an Elastic Solid* (New York: Wiley)
[18] Cottenier S, De Vries B, Meersschaut J and Rots M 2002 *J. Phys.: Condens. Matter* **14** 3283
[19] Moruzzi V L, Janak J F and Willams A R 1978 *Calculated Electronic Properties of Metals* (New York: Pergamon)
[20] Beuerle T, Hummler K, Elaässer C and Fäahnle M 1994 *Phys. Rev.* B **49** 8802
[21] Chen J, Singh D and Krakauer H 1988 *Phys. Rev.* B **38** 12834
[22] Moruzzi V L and Marcus P M 1992 *Phys. Rev.* B **46** 3171
[23] Hafner R, Spisak D, Lorenz R and Hafner J 2002 *Phys. Rev.* B **65** 184432
[24] Nonas B, Wildberger K, Zeller R and Dederichs P H 1997 *J. Magn. Magn. Mater.* **165** 137
[25] Hill P, Ali N, De Oliveria A J A, Ortiz W A, de Camargo P C and Fawcett E 1994 *J. Phys.: Condens. Matter* **6** 1761
[26] Galkin V Yu, Ali N, Fawcett F and Camargo P C de 1998 *J. Phys.: Condens. Matter* **10** 4901
[27] Sigha M and Nakamura N 1980 *J. Phys. Soc. Japan* **49** 528
[28] Dubiel S M and Zinn W 1981 *J. Magn. Magn. Mater.* **23** 214
[29] Riegel D, Büermann L, Gross K D, Luszik-Bhadra M and Mishra S N 1989 *Phys. Rev. Lett.* **62** 316